Elaboration d'un modèle thermodynamique simple de l'activité de la comète 46P/Wirtanen

Rapport du stage

Roman Ratajczak

Sous la direction: prof. J. KLINGER, E. DESVOIVRES

Grenoble 2002

Energy balance and H_2O production rate for Comet 46P/Wirtanen

Roman Ratajczak
Department of Physics
Adam Mickiewicz University
Poznan, Poland

12th July 2002

Abstract

The main purpose of this paper is to present a simple model of H_2O production rate on the surface of a spherical comet nucleus in the orbit of 46P/Wirtanen, and to compare it with observational data. The model results include the distribution of temperature on the surface. The solutions are obtained through the estimation of the energy balance. This model describes the distribution of temperature and H_2O production rate on the comet surface as a function of heliocentric distance for two cases:

- without nuclear rotation;

- fast rotation with a nucleus spin axis perpendicular to the orbital plane.

As the mixing ratio and the nucleus shape are unknown, we will consider a homogenous chemical composition of the surface layer (water ice), and the spherical nucleus shape. The nongravitational acceleration in the comet mouvement was not taken into account.

Figure 1: Image of C/2002 C1 (Ikeya-Zhang) taken March 11.77, 2002 UT [Michael Jager]

1 From antiquity until future

The earliest reliable record of cometary observations date from around 1000 BC in China, and probably from about the same time in Chaldea. But the first idea about the nature of comet is available from the time of the rise of Hellenistic natural philosophy.

The Pytagoreans (about 550 BC) considered comets to be a kind of wandering planets. Aristotle (330 BC) described comets as "dry and warm exhalations" — meteorogical phenomena in the upper atmosphere. His view was dogmatically upheld during the following millenium, when the comets were considered rather to be devil omens and signs of misfortune.

In 1578 Tycho Brache showed that the horizontal parallax of comet, which first appeared in late 1577, corresponded to a distance in excess of 230 Earth radii. The first statement that the two bright comets seen in 1680 and 1681 are one and the same before and after its perihelion passage was by Georg Dörffel, but only Isaac Newton, applying his new theory of gravitation (1687), showed that the "1680" comet moved in an eliptical orbit. In 1705 Edmond Halley computed the orbit of "1682" and predicted its return in 1758. When "Halley's Comet" was telescopically re-discovered in December 1758 by Johann Palitzsch, the road was open for a more physical approach to the study of comets.

A major revolution in cometary science took place in

2

Components Of Comets
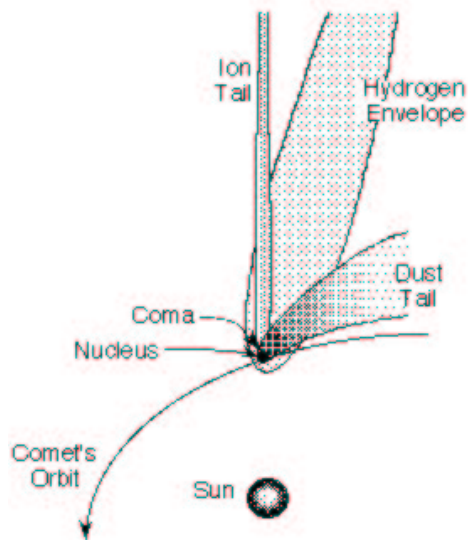
Figure 2: Comet model [C. J. Hamilton 1995]

1950-51, when Fred Whipple developped the icy conglomerate model of the cometary nucleus, and J.H. Oort explained the observed distributions of the orbits of long-period comets hypothetical "Oort cloud" surrounding the solar system at its periphery (Festou *et al.* 1993).

Actually, comets are believed to be formed during the creation of the solar system and made of the unchanged primitive material from the outer part of original solar nebula. As the observations indicate, nuclei of comets are ice-dust conglomerates with radii $\sim$ *few km* and mases $\sim 10^{10}$ to $10^{16} kg$. The mass and the heliocentric distance clearly suggest, that the material which constitute the comet nuclei is not significatly changed in the chemical and gravitational processes (maximum central pressure $\sim 10^4 N \cdot m^{-2}$). The fact that comets are some of the oldest untouched objects, makes them extremely interesting to learn about conditions during the earliest period and evolution of the solar system. In this context the future space missions to the comets will be a very important step to gain further knowledge of the orgin of comets, solar system and the univers. There are several spacecraft missions designed in the near future to study comets, e.g. the European Rosetta mission to 46P/Wirtanen.

2   Introduction

Comets are small, fragile, irregular shaped bodies consisting of frozen gases (ices — mostly H_2O) and dust. Being one of the smallest celestical bodies in the solar system, they can make the most spectacular phenomena in the sky. As a comet approaches the sun, the surface of the nucleus begins to warm and is the source of the enormous tail of luminous material (gas and dust volatiles sublimate). This tail extends for millions of kilometers from the nucleus, away from the sun (the Great Comet of 1811 has a diameter of the coma roughly equivalent to that of the sun, and the Great Comet of 1843 extend its tail $\sim$ 2 AU). For the reason of losing its volatiles, comets are said to be short-lived on a cosmological time scale.

The phenomenon, which we refer to as a comet, is composed of:

- the cometary nucleus, a kilometer-sized, irregulary shaped, solid body consisting of ices and dust;

- the coma, a gaseous and dusty atmosphere around the nucleus, which develops when it is heated as it approaches the sun and releases hydrogen in the chemical processes — the hydrogen escapes the comet's gravity, and forms a hydrogen envelope;

- the ion tail, consisting of ions which are lost from the coma and accelerated in the anti-solar direction;

- the dust tail, consisting of dust particles lost from the coma and spread along the orbit.

A model of a comet is shown on Fig.2.

Comet activity starts at heliocentric distances at least as large as 7 AU. This is due to the presence of highly volatile ices, which vaporize under the influence of solar radiation. Significant increase of nucleus activity due to H_2O sublimation, is noticeable at the distance $r_h \sim 3$ AU. Because of coma, cometary nuclei are not available for direct odservation. On the other hand, at the distance greater than 7 AU the nucleus is too small to be explored.Also the radar techniques, due to the small cross section of the nucleus and the geocentric distance dependence of the returned signal, give large dispersion of results. In addition, the presence of water vapor in the Earth's atmosphere does not permit detection of cometary H_2O from groundbased observations. Water production rate is estimated from production rates of OH radical and atomic hydrogen cre-
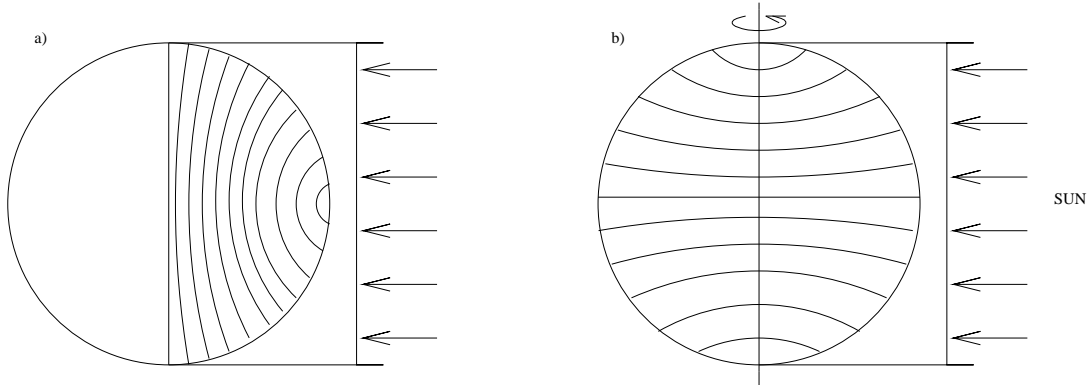
Figure 3: Comet nucleus models outline: a — without nuclear rotation; b — fast rotation with a nucleus spin axis perpendicular to the orbital plane

ated by photodisociation of H_2O molecules. As a result, many comet parameters, such as: radius, mass, nucleus rotation, surface structure, albedo, *etc.* are known only aproximately. The future space missions to the comets can resolve many problems and answer several open questions.

Periodic Comet 46P/Wirtanen is a comet discovered by C.A. Wirtanen in January 1948 as a 17th magnitude object, with the orbit typical for a Jupiter family comet (period of 6.7 years). Two close approaches with Jupiter (1972, 1984) reduced the comet's perihelion distance from 1.61 AU to 1.08 AU (recent data: perihelion distance 1.06 AU, period of 5.64 years). Actually, 46P/Wirtanen is the target of the European Space Agency's Rosetta mission. The main task of the Rosetta mission is to land on the comet and to perform several surface experiments. In addition, several atmospheric experiments are planned on the comet orbit from a heliocentric distance of 4 AU to perihelion (1.06 AU).

In the context of the Rosetta mission to 46P/Wirtanen, it is interesting to estimate the environement at the nucleus surface and in the near-nucleus coma.

3 Model description, physical parameters

In this paper we calculate H_2O production rate and distribution of temperature on the surface of 46P/Wirtanen. The model assumes a spherical nucleus shape containing one major ice component (H_2O). We use two one-dimensional models to approximate the temperature and gas production distributions on the comet nucleus surface as a function of heliocentric distance:

a) a spherical comet nucleus model without rotation, where the nucleus surface — hemisphere — is described by 90 latitudes rings;

b) the fast rotator approximation of a sphere with a nucleus spin axis perpendicular to the orbital plane, where the nucleus surface is described by 180 latitudes rings. In this case, the solar heat flux recived by the projected comet nucleus disc is averaged over the total surface of a sphere.

For every heliocentric distance the global H_2O production rate is calculated as the sum of the local outgassing rate for each surface element.

The distribution of the surface elements on the modeled nucleus is shown on Fig.3.

In our model, surface erosion, resulting from the sublimation and the grain ejection process, is not taken into account. However, these effects, depending on latitude (the higher latitudes recive less solar flux), can change the shape of the nucleus after a few orbits of the comet. The surface temperature for each of latitude rings is calculated from the energy balance equation (Delsemme 1982):

$$\frac{S(1-al)}{r_h^2} \cos z = \epsilon \sigma T^4 + L_{H_2O}^S \cdot Z_{H_2 0}; \quad (1)$$

In this equation heat transfer to deeper layers of the nucleus are neglected. The left side of the equation is the total solar flux of energy, the first term of the right

side is the termal radiation of the comet surface, and the second — heat of sublimation.

- S is the solar constant at 1 AU,

- r_h is the heliocentric distance,

- al is the nucleus albedo,

- T is the surface temperature,

- ϵ is the emissivity for reradiation,

- σ is Stefan's law constant,

- k_B is Boltzmann constant,

- z is zenith angle of the Sun.

Z_{H_2O} is the mass loss rate per unit surface area and unit time:

$$Z_{H_2O} = \frac{1}{1 + \frac{1}{\kappa}} \theta \cdot P_{H_2O}^S \sqrt{\frac{m_{H_2O}}{2\pi k_B T}}; \qquad (2)$$

where:

- m_{H_2O} is the mass of a water molecule,

- κ is a correction for the effective density of nuclear matrix:

$$\kappa = \frac{\tilde{\rho}_{H_2O}}{\tilde{\rho}_d}; \qquad (3)$$

- $\tilde{\rho}_{H_2O}$, $\tilde{\rho}_d$ are effective H_2O and dust density.

θ is sticking coefficient mesured by Haynes *et al.* and approximated by linear regresion (Enzian (1997):

$$\theta = -2.1 \cdot 10^{-3} \cdot T + 1.042 \, (T > 20K). \qquad (4)$$

$P_{H_2O}^S$ is the gas pressure of the evolving water at the surface, estimated by Clausius—Clapeyron equation:

$$P_{H_2O}^S = \vartheta \cdot e^{\left[\frac{-E}{k_B \cdot T}\right]}; \qquad (5)$$

where:

- ϑ is the parameter corresponding to a chatacteristic pressure:

$$\vartheta = 3.56 \cdot 10^{12} Pa; \qquad (6)$$

- E is the activation energy:

$$\frac{E}{k_B} = 6141.667 K. \qquad (7)$$

$L_{H_2O}^S$ is the latent heat of sublimation for water ice calculated according to experimental data by Delsemme and Miller (1971):

$$L = 2.886 \cdot 10^6 - 1116 \cdot T [J \cdot kg^{-1}]. \qquad (8)$$

The cometary matrix albedo and the emissivity for reradiation are not well known parameters. In indirect measurement, the albedo was estimated as $0.04 \leq al \geq 0.15$ (Levasseur-Regourd 1998).

The observations of 46P/Wirtanen with the HST estimate a mean effective radius of $0.58 km$ for the geometric albedo of 0.04 (Lamy 1996).

The emissivity for reradiation for non-metalic material is between 0.85 and 0.95 (Kuchling 1985).

In Table I we present the most important physical parameters used for this work.

4   Results

We present the results of outgasing and the distribution of temperature for two models of comet 46P/Wirtanen assuming a spherical nucleus shape, starting at aphelion (5.13 AU) to perihelion (1.06 AU).

Our model considers the energy balance as a function of heliocentric distance and nucleus latitude, involving:

- thermal radiation;

- heat expance due to sublimation from a surface of pure H_2O ice.

We also assume that the total surface of 46P/Wirtanen is active.

The most important result of our simply simulation is

TABLE I		
Semimajor axis	a	3.099289 AU
Orbit eccentricity	e	0.656770
Nucleus radius	R	600 m
Bond albedo	al	0.04
Infrared emissivity	ϵ	0.9
Bulk density	κ	1
Spin axis		Perpendicular to orbital plane

Table 1: Physical input parameters

the determination of limit H_2O production rate. In addition we present several others parameters obtained through the simulation.

The results of calculations are shown on figures 4 — 29:

- Figures 4 — 9 show evolution of two terms of energy and their sum versus heliocentric distance for 3 different latitudes.

- In figures 10 and 11 we compare the surface temperature versus heliocentric distance.

- The evolution of surface temperature versus zenith angle of the Sun for 4 heliocentric distance are shown on figures 12 — 15. Figures 16 and 17 are comparison of two considered models.

- In the figures 18 and 19 water production rate (Q_{H_2O}) for 3 different latitudes is shown as a function of heliocentric distance.

- Figures 20 and 21 show energy balance versus temperature for subsolar point; and 22, 23 — for $z = 45°$.

- Total evolution of termal radiation, sublimation heat and their sum versus heliocentric distance are illustrated on figures 24 — 27.

- Figures 28, 29 are comparison of total energy balance and total water production rate versus heliocentric distance for two considered models.

5   Comparison with observational data

There are several estimation methods of the water production rate. One of them is the estimation from OH radical and atomic hydrogen production rates, using narrowband photometry. Other metod — from an analysis of the Lyman-alpha emission of the hydrogen enveloppe (SWAN experiment on board of the SOHO spacecraft). Another method of estimating water production — by using an empirical relation between Q_{H_2O} and the heliocentric magnitude m_h, is given by Jorda (1995):

$$log(Q_{H_2O}) = 30.78(\pm 0.25) - 0.265 m_h. \quad (9)$$

Observations of the OH radical performed by A'Hearn in 1991 (A'Hearn *et al.* 1996), derived a water production rate of $Q_{H_2O} = 1.2 \cdot 10^{28}[molecules \cdot s^{-1}]$ —

Haser model, or $Q_{H_2O} = (1.3 - 2.5) \cdot 10^{28}[molecules \cdot s^{-1}]$ — model of Combi and Delsemme (Rickman, Jorda 1998). The H_2O production rate, determined by SWAN instrument on board SOHO (Lyman-α photometer), is $\sim 1.6 \cdot 10^{28}[molecules \cdot s^{-1}]$ just before perihelion in 1997 (Bertaux *et al.* 1997). The visual lightcurves of perihelion passage in 1986 and 1991 yield a production rate of $4 \cdot 10^{28}[molesules \cdot s^{-1}]$ (Jorda, Rickman 1995).

As the figures show, our computations give total H_2O production rate at perihelion:

- $9.4 \cdot 10^{27}[molecules \cdot s^{-1}]$ non-rotating nucleus model;

- $9.8 \cdot 10^{27}[molecules \cdot s^{-1}]$ fast rotator approximation.

The energy per unit of time for non-rotating model is twice as big as for the fast rotator approximation. However, we can assumed that the total H_2O production magnitude is the same for two considered cases. This is due to the fact, that the solar heat flux recived by projected comet nucleus disc, for the fast rotator approximation, is averaged over the total surface of a sphere. For a comet nucleus radius of $600m$ our models cannot explain the measurements. Thus, one need to find other mechanisms that are able to increase the water flux.

6   Conclusions

As the observations indicate, 46P/Wirtanen has a radius $\sim 600m$, and is very actively outgasing. The observed production rate of $4 \cdot 10^{28}[molesules \cdot s^{-1}]$ (Jorda, Rickman 1995) cannot be explained by free surface sublimation of water ice from a comet nucleus having a mean effective radius of about $600m$. In addition, because of several approximations, e.g. homogenous chemical composition (H_2O) and total surface activity, our model is not very realistic. The real situation may have further complications, however our models give the upper limit of H_2O production rate for nucleus radii of $600m$. In the other hand, the energy balance clearly indicate that exist other mechanisms able to increase the water flux.

Other explanation of observed H_2O production rate — water-ice particles are blown off the surface and sublimate outside, increasing the effective area of sublimation (Benkhoff 1999).

Fig. 30. shows increase in total water production rate assuming a radius of $1200m$.
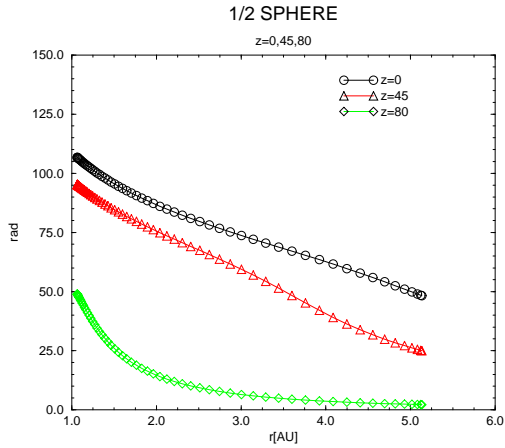
Figure 4: Termal radiation $[W \cdot m^{-2}]$ versus heliocentric distance [AU]; non-rotational model ($z = 0°, 45°, 80°$, solar flux is projected on the flat surface)
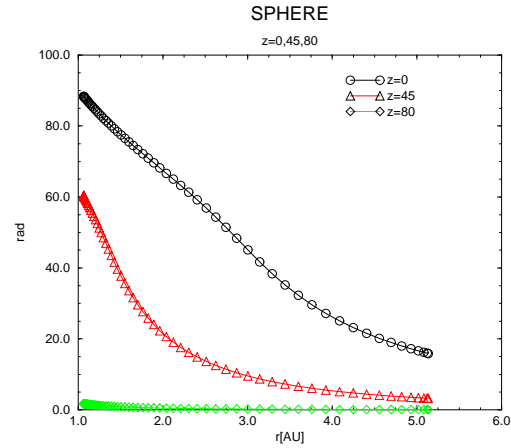
Figure 5: Termal radiation $[W \cdot m^{-2}]$ versus heliocentric distance [AU]; fast rotator approximation ($z = 0°, 45°, 80°$, solar flux is projected on the flat surface)
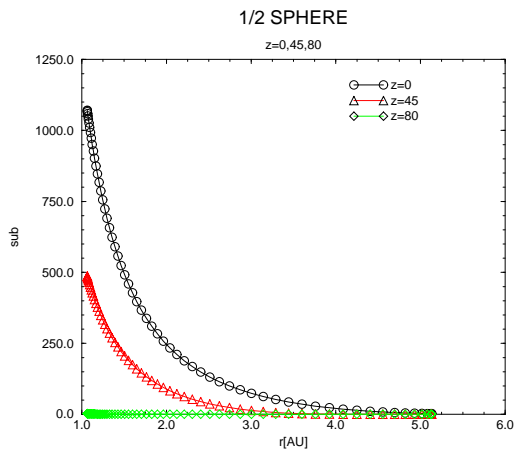
Figure 6: Sublimation heat $[W \cdot m^{-2}]$ versus heliocentric distance [AU]; non-rotational model ($z = 0°, 45°, 80°$, solar flux is projected on the flat surface)
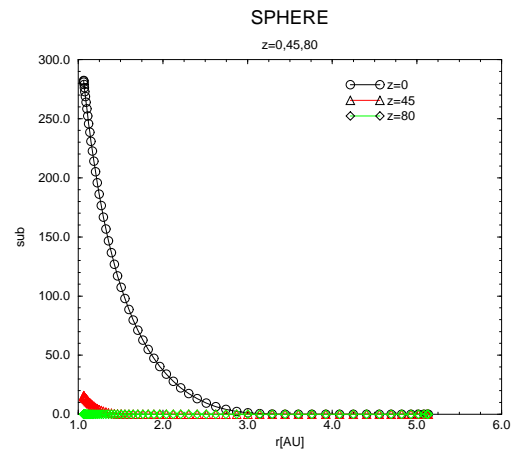
Figure 7: Sublimation heat $[W \cdot m^{-2}]$ versus heliocentric distance [AU]; fast rotator approximation ($z = 0°, 45°, 80°$, solar flux is projected on the flat surface)
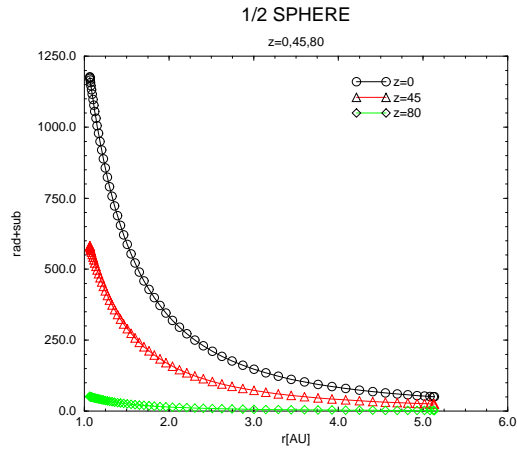
Figure 8: Sum of termal radiation and sublimation heat $[W \cdot m^{-2}]$ versus heliocentric distance [AU], non-rotational model ($z = 0°, 45°, 80°$, solar flux is projected on the flat surface)
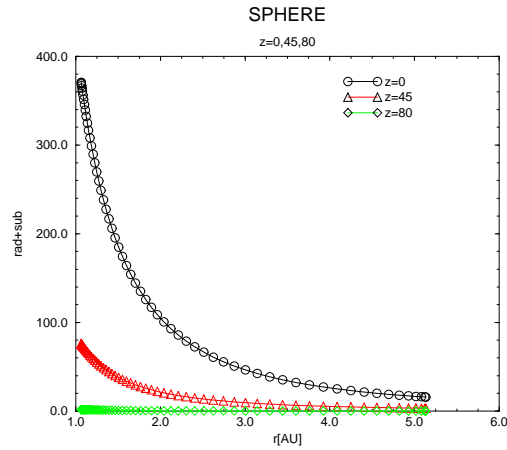
Figure 9: Sum of termal radiation and sublimation heat $[W \cdot m^{-2}]$ versus heliocentric distance [AU]; fast rotator approximation ($z = 0°, 45°, 80°$, solar flux is projected on the flat surface)
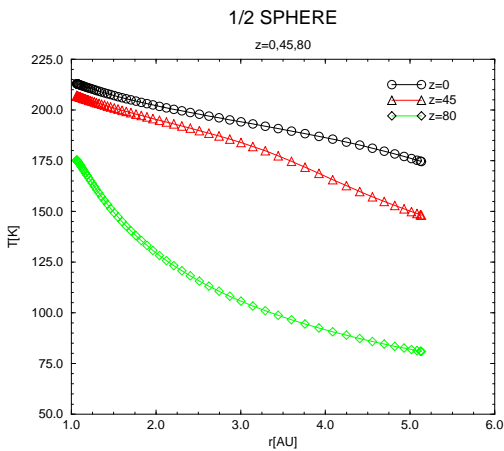
Figure 10: Evolution of surface temperature $[K]$ vs heliocentric distance [AU]; non-rotational model ($z = 0°, 45°, 80°$, solar flux is projected on the flat surface)
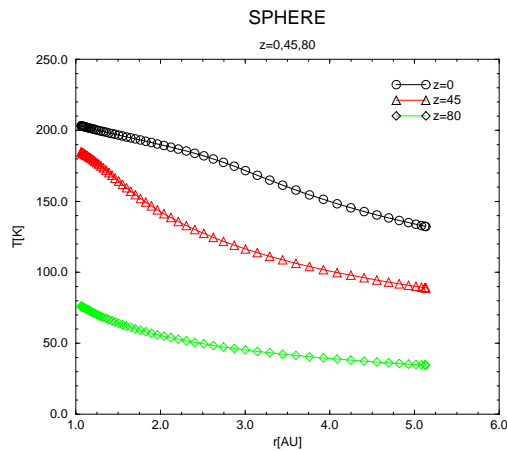
Figure 11: Evolution of surface temperature $[K]$ versus heliocentric distance [AU]; fast rotator approximation ($z = 0°, 45°, 80°$, solar flux is projected on the flat surface)
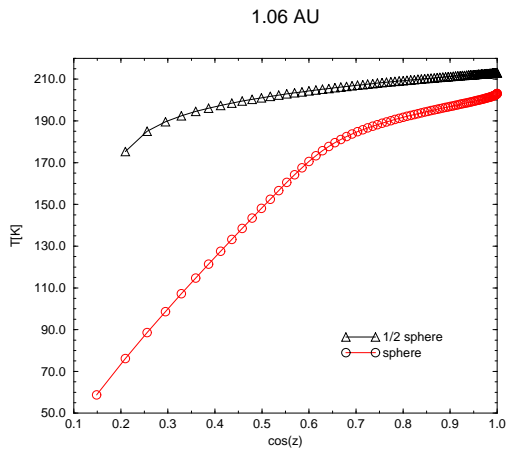
Figure 12: Evolution of surface temperature $[K]$ versus $cos(z)$ (z — zenith angle of the sun) for heliocentric distance 1.06AU (perihelion)
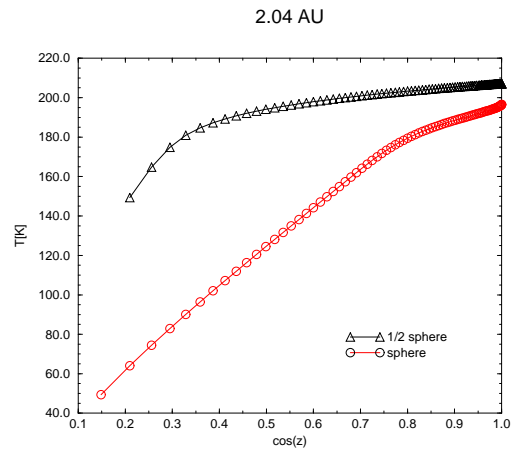
Figure 13: Evolution of surface temperature $[K]$ versus $cos(z)$ (z — zenith angle of the sun) for heliocentric distance 3.60AU
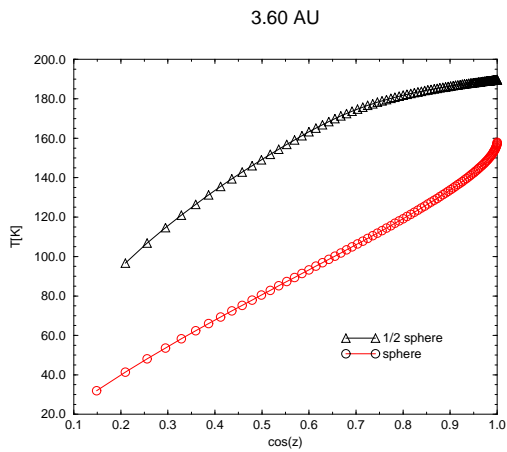
Figure 14: Evolution of surface temperature $[K]$ versus $cos(z)$ (z — zenith angle of the sun) for heliocentric distance 2.4AU
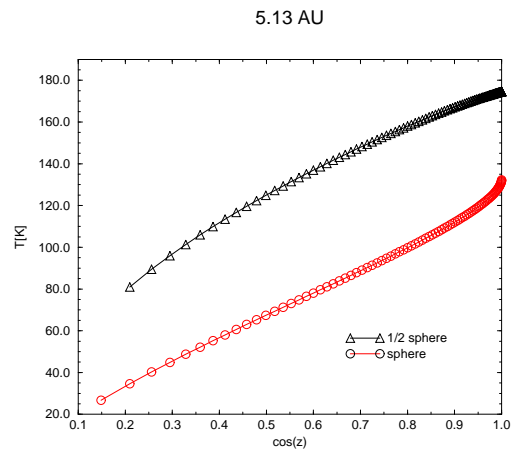
Figure 15: Evolution of surface temperature $[K]$ versus $cos(z)$ (z — zenith angle of the sun) for aphelion (5.13AU)
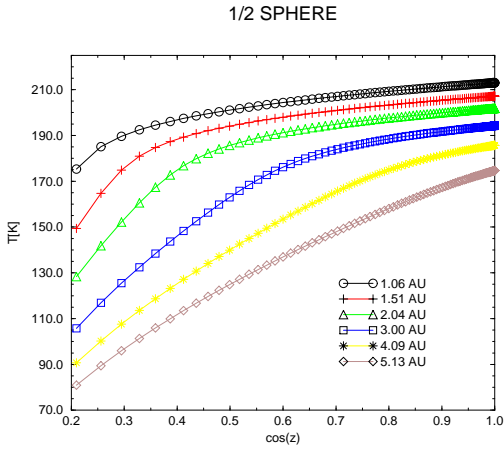
Figure 16: Evolution of surface temperature $[K]$ versus $\cos(z)$ (z — zenith angle of the sun) for 6 different distances (non-rotating model)
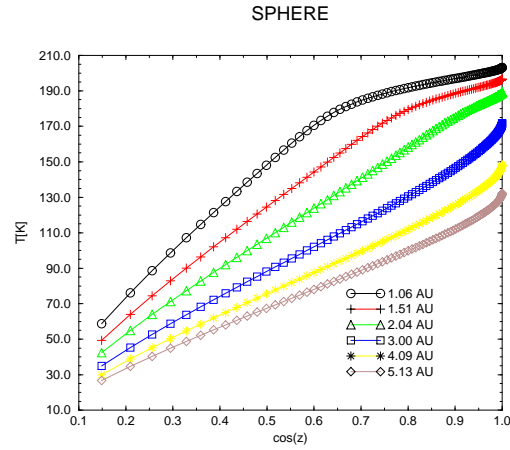
Figure 17: Evolution of surface temperature $[K]$ versus $\cos(z)$ (z — zenith angle of the sun) for 6 different distances (fast rotator approximation)
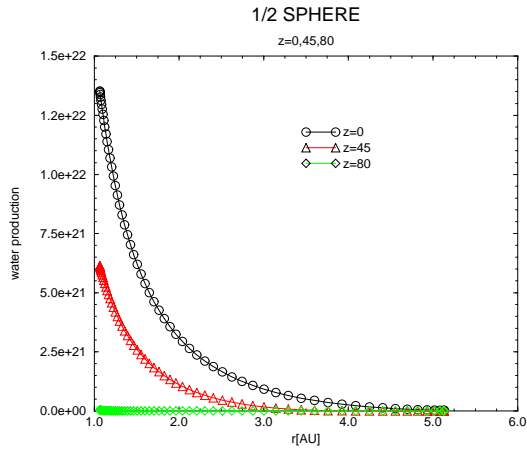
Figure 18: Water production rate $[molecules \cdot s^{-1} \cdot m^{-2}]$ versus heliocentric distance [AU] (non-rotating model, $z = 0°, 45°, 80°$, solar flux is projected on the flat surface)
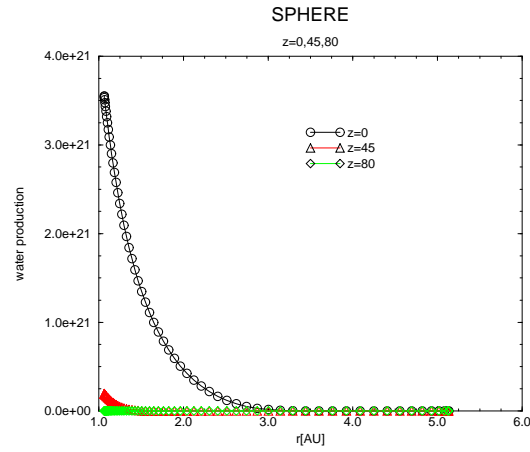
Figure 19: Water production rate $[molecules \cdot s^{-1} \cdot m^{-2}]$ versus heliocentric distance [AU] (fast rotator approximation, $z = 0°, 45°, 80°$, solar flux is projected on the flat surface)
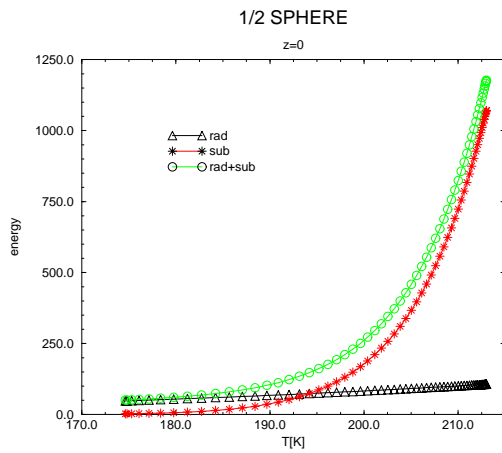
Figure 20: Energy balance $[W \cdot m^{-2}]$ versus temperature [K] for subsolar point, non-rotating model
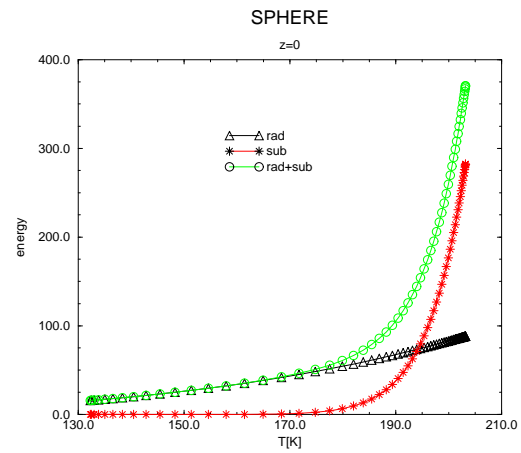
Figure 21: Energy balance $[W \cdot m^{-2}]$ versus temperature [K] for subsolar point, fast rotator approximation
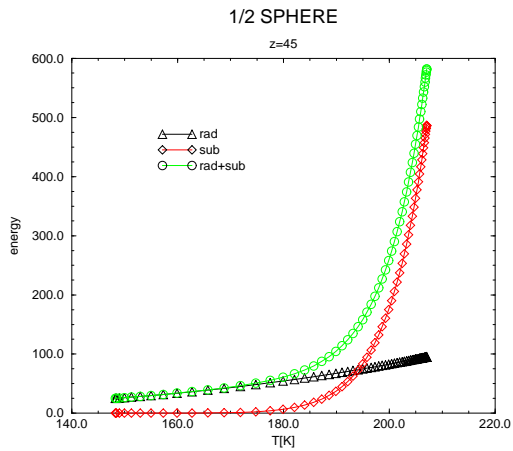
Figure 22: Energy balance $[W \cdot m^{-2}]$ versus temperature [K] for $z = 45°$, non-rotating model
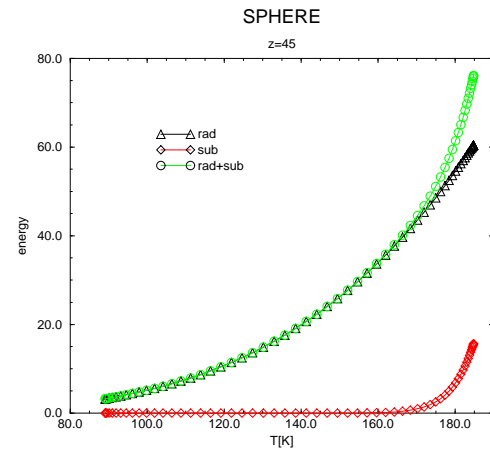
Figure 23: Energy balance $[W \cdot m^{-2}]$ versus temperature [K] for $z = 45°$, fast rotator approximation
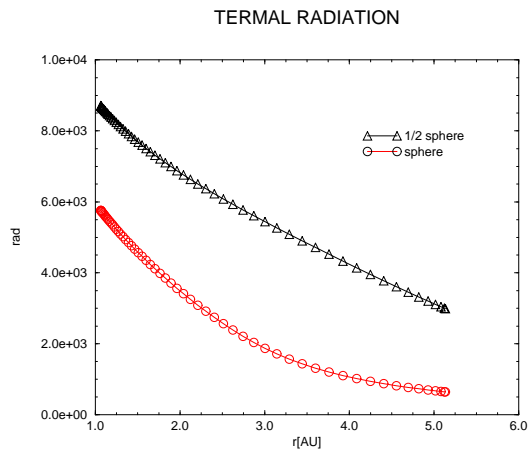
TERMAL RADIATION

Figure 24: Total termal radiation [W] versus heliocentric distance [AU]
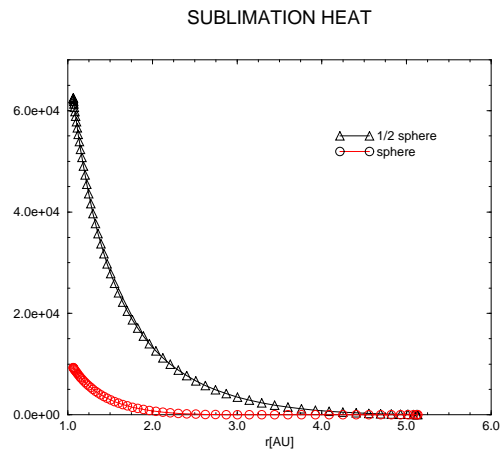
SUBLIMATION HEAT

Figure 25: Total sublimation heat [W] versus heliocentric distance [AU]

1/2 SPHERE
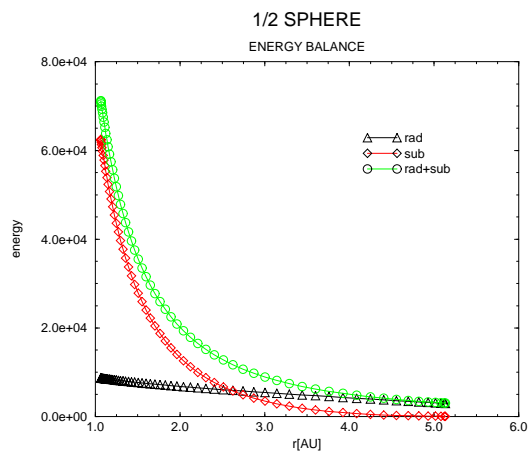
Figure 26: Total energy balance [W] versus heliocentric distance [AU]; non-rotating model

SPHERE
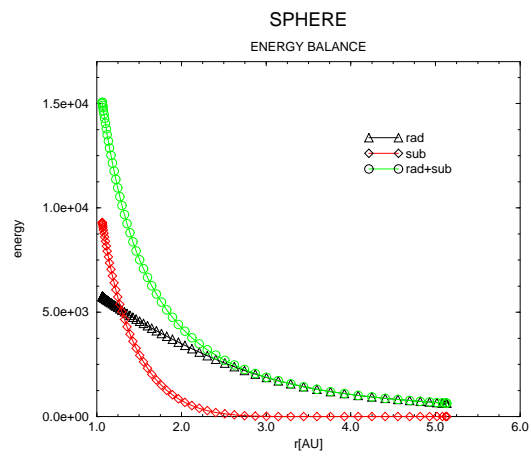
Figure 27: Total energy balance [W] versus heliocentric distance [AU]; fast rotator approximation

COMPARISON OF ENERGY
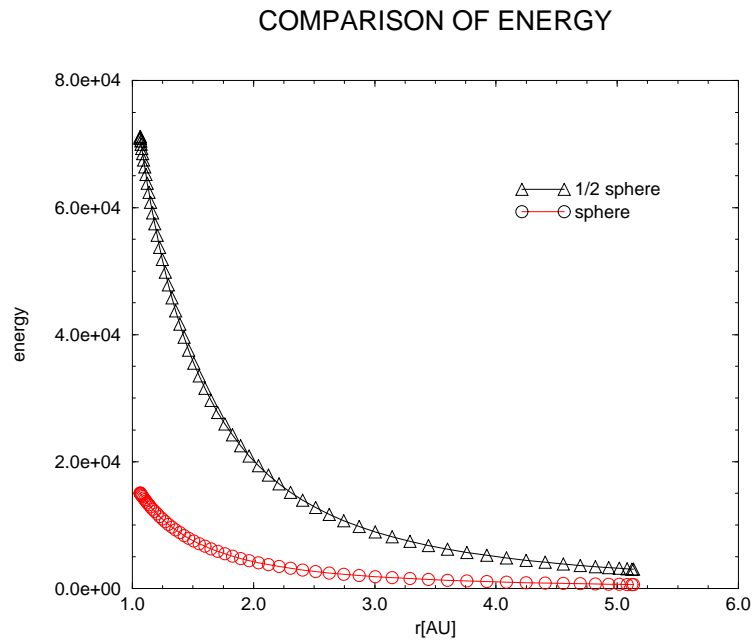
Figure 28: Comparison of energy balance for two models — total energy [W] versus heliocentric distance [AU]

TOTAL WATER PRODUCTION
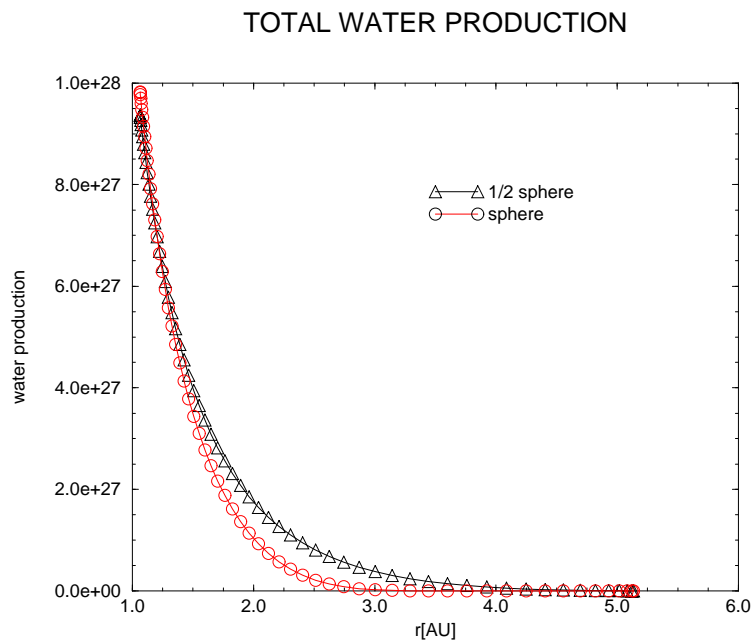
Figure 29: Total water production rate [$molecules \cdot s^{-1}$] versus heliocentric distance [AU] — comparison of two considered models
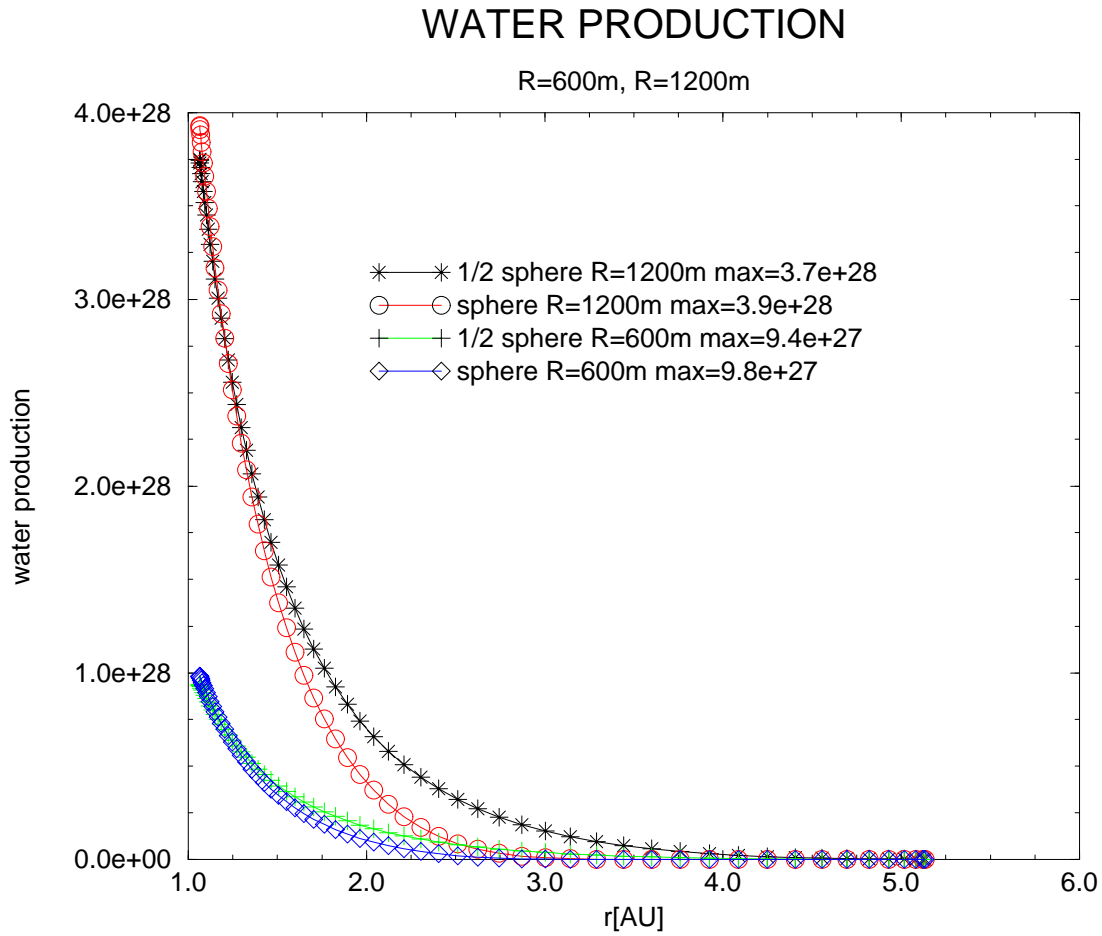
Figure 30: Symulation of water production rate [$molecules \cdot s^{-1}$] versus heliocentric distance [AU] for nucleus radii R=1000m (two models) and comparison with considered models

7   References

A'HEARN, M. F., BERTAUX, J. L., FELDMAN, P. D., PARKER, J. WM., SCHULZ, R., STERN, S. A., WEINTRAUB, A. D., (1996) HST/FOS UV Observations of Chiron and Wirtanen. *American Astronomical Society*, **Vol. 28**, 1083.

BENKHOFF, J., (1999) Energy balance and the gas flux from the surface of comet 46P/Wirtanen. *Planet.Space Sci.*, **Vol. 47**, 735-744.

BERTAUX, J.C., COSTA, J., MÄKINEN, T., QUÉMERAIS, E., LALLEMENT, R., KYRÖLÄ, E., SCHMIDT, W., (1997) Lyman-alpha Observations of 46 P/Wirtanen (1998) with SWAN on SOHO: H_2O Production rate near 1997 perihelion. *Presented at Workshop on the Rosetta Targets, Napoli, 1997.*

COMBI, M. R., DELSEMME, A. H., (1980) Neutral cometary atmospheres. I - an average random walk model for photodissociation in comets. *Astrophysical Journal*, **Vol. 237**, 633-640.

DELSEMME, A. H., MILLER, D. C., (1971) Physico-chemical phenomena in comets-III. The continuum of comet Burnham (1960 II). *Planet.Space Sci.*, **19**, 1229-1257.

DELSEMME, A. H. (1982) Chemical composition of cometary nuclei, in *Comets*, L.L. Wilkening, 85-130, *The University of Arizona Press, Tucson, 1982.*

DESVOIVRES, E., (1999) Modélisation de la dynamique des fragments cométaires - Application à la comète C/1996 B2 Hyakutake. *Doctoral thesis, Univ. Joseph Fourier, Grenoble I.*

ENZIAN, A., (1997) Modélisation multidimensionnelle du comportement thermodynamique des noyaux de comètes. *Doctoral thesis, Univ. Joseph Fourier, Grenoble I.*

ENZIAN, A., KLINGER, J., SCHWEHM, G., WEISSMAN, P. R., (1999) Temperature and Gas Production Distributions on the Surface of a Spherical Model Comet Nucleus in the Orbit of 46P/Wirtanen. *Icarus*, **Vol. 138**, 74-84.

FESTOU, M. C., RICKMAN, H., WEST, R. M., (1993) Comets. Scientific preprint. *European Southern Observatory.* No. 960.

HAMILTON, C. J., (1995) Views of the Solar System. *Privacy Statement http://www.solarviews.com*

HASER, L., (1957) Distribution d'intensité dans la tête d'une comète. *Bull. Acad. R. Sci. Liège*, **Vol. 43**, 740-750.

HAYNES, D. R., TRO, N. J., GEORGE, S. M., (1992) Condensation and evaporation of H_2O on ice surfaces. *J.Phys.Chem.*, **96**, 8502—8509.

JORDA, L., (1995) Atmosphères cométaires: interprétation des observations dans le visible et comparaison avec les observations radio. *Doctoral thesis, Observatoire de Paris-Meudon, Université de Paris VII.*

JORDA, L., RICKMAN, H., (1995) Comet P/Wirtanen, summary of observational data. *Planet. Space Sci.*, **Vol. 43**, 575-579.

KUCHLING, F., (1985) Taschenbuch der Physik. *Verlag Harri Deutsch, Thun and Frankfurt.*

LAMY, P. L., (1996) Comet 46P/Wirtanen. *IAU Circ.*, 6478.

LEVASSEUR-REGOURD, A. C., (1998) Zodiacal light, certitudes and questions. *Earth, Planet. Space*, **50**, 607-610.

RICKMAN, H., JORDA, L., (1998) Comet 46P/Wirtanen, the target of the Rosetta mission. *Adv. Space Res.*, **Vol. 21**, No. 11, 1491–1504.

SAMARASINHA, N. H., MUELLER, B. E. A., BELTON, M. J. S., (1996) Comments on the rotational state and non-gravitational forces of comet 46P/Wirtanen. *Planet. Space Sci.*, **Vol. 44**, No. 3 275-281.